Urban Climate 58 (2024) 102198

Contents lists available at ScienceDirect

Urban Climate

journal homepage: www.elsevier.com/locate/uclim

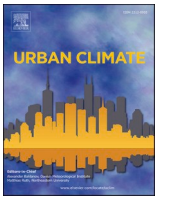

Effects of the urban development on the near-surface air temperature and surface energy balance: The case study of Madrid from 1970 to 2020

J. Carbone [a,*], B. Sanchez [b], C. Román-Cascón [c], A. Martilli [b], D. Royé [d], C. Yagüe [a]

[a] Departamento de Física de la Tierra y Astrofísica, Universidad Complutense de Madrid, 28040 Madrid, Spain
[b] Atmospheric Modelling Unit, Environmental Department, CIEMAT, 28040 Madrid, Spain
[c] Departamento de Física Aplicada, Facultad de Ciencias del Mar y Ambientales, INMAR, CEIMAR, Universidad de Cádiz, 11510 Cádiz, Spain
[d] Climate Research Foundation (FIC), 28013 Madrid, Spain

ARTICLE INFO

Keywords:
Urban climate
Urban growth
Near-surface air temperatures
Surface energy balance
Turbulence
Heatwave
Stable atmospheric conditions
Madrid

ABSTRACT

The aim of the present study is to examine the impact of Madrid's urban growth over the last 50 years (1970–2020). We conduct a modelling study using WRF-ARW with the multilayer urban parameterization BEP-BEM, in which different urban parameters have been incorporated at each point within the model's inner domain according to urban expansion from 1970 to 2020. Two scenarios of important societal interest with different meteorological conditions are selected for this study: a period of intense heatwave during the summer season and a short period of strongly stable atmospheric conditions in winter, both in 2020. The results show that in areas where the urban fraction becomes greater an increase in near-surface air temperature is found for both simulated periods, especially during the night. The urbanization modifies the surface energy balance and turbulent transport in Madrid and its surroundings. It leads to a decrease in latent heat flux due to the high impermeability and reduced vegetation in urban areas. Additionally, the urban areas with a higher density of buildings have a high heat capacity, increasing heat flux storage during the day through solar radiation absorption. This stored energy is released at night, exacerbating the increase in nighttime near-surface air temperature in both periods.

1. Introduction

The proportion of the world's population living in urban areas has experienced a significant increase over the past 50 years, rising from 37 % to 56 %, with projections indicating that this trend will continue, reaching 60 % by the year 2030 (Gerland et al., 2022). Future urbanization will amplify the projected air temperature changes in cities that can be as large as the global warming signal (AR6 – IPCC, 2022), which entails that the risk faced by people associated with climate change and urbanization increases (Chapman et al., 2017). This growth in urban population increases the demand for services, housing, and utilities, and changes of land cover and infrastructure features modulate local and regional weather and climate. In the last decades several studies have been conducted to understand how urban meteorology and climate is affected by various factors, including the thermal properties of the construction materials used in buildings, the asphalt on streets, other impermeable surfaces (Oke, 1988), and the increase in anthropogenic heat

* Corresponding author.
E-mail address: jcarbone@ucm.es (J. Carbone).

https://doi.org/10.1016/j.uclim.2024.102198
Received 8 February 2024; Received in revised form 17 October 2024; Accepted 1 November 2024
Available online 22 November 2024

generated directly by human activities (Sailor, 2011; Zhang et al., 2013). The main outcome of those studies is that all these factors give rise to unique urban climates from micro to regional scales (Arnfield, 2003; Yan et al., 2016; Zhou et al., 2017; Sharma et al., 2020).

Cities have a multitude of interactions with the overlying atmosphere that modify the exchange of heat, momentum, and moisture between the surface and the lower atmosphere (Grimmond, 2007). This is due to the highly variable and different thermal characteristics of built-up areas compared to the surrounding rural areas, dynamic interaction with the mean flow due to the roughness of these cities, and the lack of vegetation that reduces the transfer of moisture from the ground to the atmosphere (Myrup, 1969; Mills et al., 2022). These urban surfaces redistribute heat differently than rural areas due to differences in the Surface Energy Balance (SEB) (Schlünzen et al., 2023), often resulting in higher temperatures in these urban zones (Landsberg, 1981; Stewart and Oke, 2012). This phenomenon is the main cause of the Urban Heat Island (UHI) effect and remains one of the most significant consequences of urbanization (Vitanova et al., 2021), which is further exacerbated by the heat generated by anthropogenic activities such as traffic, industry, the use of electrical appliances, ventilation systems, and air conditioning. Especially in summer, these activities contribute to increase air temperatures (Salamanca et al., 2012; Maqueda et al., 2020). The most remarkable characteristic is that the cooling rate is reduced during the afternoon/night, causing the minimum temperature to be higher in urban areas than in nearby rural areas (Oke and Cleugh, 1987; Chow and Svoma, 2011). This very noticeable UHI effect during the night can result in additional warming of the urban area by up to 7–10 °C (Lokoshchenko, 2014).

This study focuses on Madrid region, located in the center of the Iberian Peninsula, which is recognized as one of the most vulnerable places to the current climate change situation (IPCC, 2021). This vulnerability is especially pronounced due to the prevalence of stable synoptic conditions in summer associated with heatwaves, the intensities and duration of which have increased in recent years (Rasilla et al., 2019; Lorenzo et al., 2021; Barriopedro et al., 2023). Heat-related mortality has been identified as one of the key climate extremes posing a risk to human health and highlights the urgency for strong mitigation and adaptation to reduce impacts on human lives (Vicedo-Cabrera et al., 2021; Tobias et al., 2023; Lüthi et al., 2023).

Madrid, one of the major cities in Europe, experiences a significant UHI effect in its metropolitan area, with average magnitudes ranging between 4 °C and 6 °C (Yagüe et al., 1991; Salamanca et al., 2012; Rasilla et al., 2019; Ezpeleta and Royé, 2021; Núñez-Peiró et al., 2021). Moreover, the urban area of the greater Madrid (including the municipality and all the surrounding satellites cities) experienced a strong sprawling in the last 50 years. Between 1970 and 2020 the population of the region has doubled, but the extension of the built surfaces has increased by a factor 5 (López de Lucio, 2003; Muñoz, 2003; National Institute of Statistics of Spain, 2023). This extraordinary urban development is the result of a number of drivers other than population growth, including a strong demand for first and second homes supported by an increase in wealth combined with low mortgage interest rates, and an improved transportation network (EEA, 2006; García-Palomares, 2010). This effect is a consequence of the high population density, which requires a substantial number of buildings, infrastructure, and energy resources. Consequently, temperatures are significantly elevated within the first few

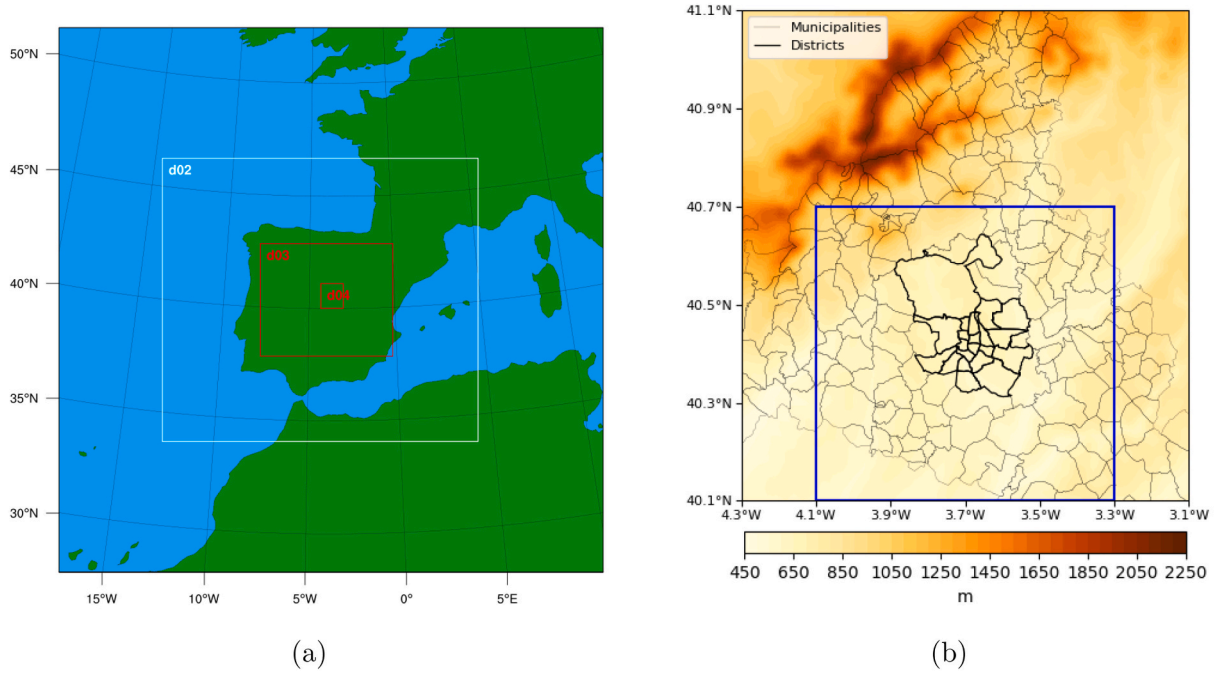

Fig. 1. (a) The computational domain with four nested grids. (b) The terrain height for the inner domain. The blue domain is the area where land use and land cover have been modified according to urban expansion from 1970 to 2020, which corresponds to the most populated area. (For interpretation of the references to colour in this figure legend, the reader is referred to the web version of this article.)

meters of the atmosphere compared to the surrounding areas, due to alterations in the heat capacity and thermal conductivity of these urban surfaces, especially during anticyclonic situations (Yagüe et al., 1991; Salamanca et al., 2012).

The UHI intensity or time series analysis of long-term temperature data (minimum or maximum temperatures) from a single meteorological station or a network of stations, has been traditionally used as an indicator to assess the effects of changes in land use and land cover (LULC) (Oke, 1973; Landsberg, 1981; Gallo et al., 1996; Maqueda et al., 2020). However, interpreting these variables can be challenging, as they depend on how urban and rural areas are defined. Typically, previous analyses have focused solely on maximum values near the urban core, neglecting to examine these impacts in residential areas, which frequently represent the predominant land use in urban environments. Hence, the main objective of this work is to assess the impact of urban development in the city of Madrid and its surroundings on the local weather, separated from the effect caused by the global warming signal. To achieve this, we analyze the impact of urban growth and assess how "current" events would have behaved under lower urbanization conditions. In this way, two short periods representatives of different current weather situations are selected: an intense heatwave event (August 2020) and a strongly stable atmospheric conditions in winter (February 2020), and we use the mesoscale model WRF-ARW with the multilayer BEP-BEM scheme to represent urban areas (Martilli et al., 2002; Salamanca et al., 2010) in order to capture the effects of urban development in our simulations (Chen et al., 2011). The methodology followed consists in modifying LULC using realistic maps of the urban development of the Madrid region in 1970 and 2020.

2. Data and methodology

2.1. Site description

According to the Köppen-Geiger classification (Kottek et al., 2006), Madrid has a Mediterranean climate bordering the semi-arid class (Csa – BSk), with hot summers and cold winters. Precipitation tends to concentrate in spring and autumn, while cloudless days are mostly observed in summer. Regionally, its climate is slightly influenced by the presence of the Central System (Fig. 1). Madrid is in the center of the Iberian Peninsula, on a plateau at an elevation of approximately 600 m a.s.l., with a mountain range (Sierra de Guadarrama) at the NW, reaching heights of up to 2428 m a.s.l. The core of the city is bounded by two small valleys oriented in a NNW-SSE direction, crossed by the Manzanares and Jarama rivers. This influences the predominant wind direction, which generally blows from NE during the night and SW during the day, creating a temperature gradient from north to south, with cooler conditions in the north and warmer conditions in the south of the metropolitan area (Fernández García et al., 1996). The difference in elevation between the bottom of the valleys and the hill where the old city center is located is approximately 100 m.

In the municipality of Madrid, more than 3.3 million people reside with a population density of 5418 hab km^{-2}, while the metropolitan area of Madrid has a population of 6.7 million, with a significant increase in the last decades (National Institute of Statistics of Spain, 2023). The rural areas surrounding Madrid are typically Mediterranean in nature, although influenced by altitude and the distance from the sea, featuring a mix of farmland, shrubland, and evergreen trees, especially near the mountains. Regarding urban land cover classification, the local climate zone (LCZ) scheme is commonly used to divide the landscape into regions of uniform surface cover, structure, material, and human activity (Stewart and Oke, 2012). Overall, in Madrid there is a prevalence of compact midrise (LCZ 2) and open midrise (LCZ 5) (Fig. 3). The large low-rise urban class (LCZ 8) is also substantially present in the southwestern periphery.

2.2. Simulated periods description

As commented before, two periods were simulated to investigate the effect of the urban expansion: a heatwave in summer and stable atmospheric conditions in winter, both of a present day climate, to isolate the impact of the urban expansions from the global climate change signal.

2.2.1. Summer period

To select this period, we have defined a heatwave as an episode of at least 3 consecutive days, during which at least 10 % of the considered stations display maximum temperatures above the 95th percentile of their daily maximum temperature series for the months of July and August for the 1971–2000 period. This is the standard definition used by the Spanish State Meteorological Agency (AEMET, 2022). The simulated period comprises from August 4th at 1200 UTC to August 10th at 0000 UTC (considered by AEMET as a heatwave), focusing on the results from 0000 UTC of the 5th (12 h of spin up). At the synoptic scale, high-pressure systems dominated over the Iberian Peninsula during the period, as typical in the region in summer. A Mediterranean anticyclone was also present,

Table 1
Observational data of temperature (T), wind speed (WS), and relative humidity (RH) for both simulated periods at the meteorological station located in Plaza Elíptica (air quality monitoring station of the Madrid city network (Data Air Quality Network)).

PERIOD	T (°C)			WS (m/s)			HR (%)		
	mean	max	min	mean	max	min	mean	max	min
Summer	30.7	39.1	22.2	1.03	2.07	0.50	31.4	53.0	17.0
Winter	8.8	15.4	3.7	0.85	2.25	0.51	76.6	95.0	29.0

accompanied by the influence of a subtropical air mass that affected the central and eastern regions of the peninsula, leading to the peak temperatures. The NCEP-NCAR reanalysis composites from this period are included in Fig. A.1 of supplemental material. An overview of the meteorological conditions during this period is provided in Table 1. Data from the meteorological station located at Plaza Elíptica were used (air quality monitoring station of the Madrid city network (Data Air Quality Network)). Table 2 provides detailed information about the location of this station, the urban fraction, as well as the LCZ based on the categories defined by Stewart and Oke (2012).

2.2.2. Winter period

The period of strongly stable winter atmospheric conditions in 2020 was simulated between February 19th at 1200 UTC to February 25th at 0000 UTC, and results are analyzed starting from 0000 UTC of the 20th (12 h of spin up). These days were characterized by a high-pressure blocking system situated over western Europe (Fig. A.2 of the supplemental material), with a weak surface-pressure gradient in the central area of the Iberian Peninsula. This situation favours very low wind conditions, especially during the evening transitions (Román-Cascón et al., 2023). An overview of the meteorological conditions during this period is provided in Table 1.

2.3. Model setup

WRF-ARW version 4.3 has been used to perform the simulations, with four nested domains (27 km, 9 km, 3 km, 1 km) centered on the city center (40° 25′ 0.4” N and 3° 42′ 13.6” W) and including most of the close mountain ridge (Fig. 1). The analysis focused on the innermost domain, which has 111 × 123 grid points with the horizontal resolution of 1 km. In the vertical, a constant resolution of approximately 5 m is used for the lowest 10 vertical levels (i.e., up to 50 m a.g.l.), and then the resolution is progressively stretched for a total of 57 numerical grid vertical levels (33 of them in the lowest 1 km), until 20 km. This provides high vertical resolution near the surface, allowing for an accurate reproduction of vertical profiles of meteorological and turbulent variables in the urban area, which is very important for this study. The physical parameterizations used in the simulations include the Rapid Radiative Transfer longwave radiation scheme (Mlawer and Clough, 1997), Dudhia shortwave radiation scheme (Dudhia, 1989), a revised version of Monin-Obukhov surface layer scheme (Monin and Obukhov, 1954; Jiménez et al., 2012), and WRF Single-Moment-Microphysics scheme (Hong et al., 2004). Turbulence in the planetary boundary layer is parameterized based on the Bougeault and Lacarrere turbulent scheme (Bougeault and Lacarrere, 1989) and rural land surface, and soil heat and moisture fluxes are treated by the Noah Land Surface Model (Chen and Dudhia, 2001).

We focus our analysis on the two selected periods that span 5 days with a 12-h spin-up time. Using two different meteorological conditions periods allows to estimate the influence of the urban expansion in different synoptic conditions over the urban climate. In order to assess the impact of the current extent and nature of Madrid’s urban growth over the last 50 years (1970–2020), we conducted paired simulations with identical meteorology for each period (initial and boundary conditions are derived from the NCEP-FNL data at 0.25° resolution every 6 h) driven by two LULC scenarios in 1970 and 2020. These databases (Uhl et al., 2023) include urban parameters such as urban fraction, mean building height (H_{mean}), building plan area density (λ_p) and density of building surfaces (λ_b), which have been computed for each point within the inner domain. The urban fraction is derived from the urban morphological data described in section 2.4. This data has a horizontal resolution of 100 m, that is then aggregated up to the resolution of the finer domain (1 km). In particular, the urban fraction at 1 km resolution is equal to the fraction of points of the morphological dataset (100 m × 100 m) with building plan area density greater than zero. Considering that within a 1 km^2 grid cell there are 100 points, the estimate is expected to be quite accurate. All the other morphological parameters (λ_p, λ_b, H_{mean} and distribution) are derived from the morphological dataset by averaging them, and are given point by point. This provides a realistic view of LULC for these decades, and it allows us to represent urban development, as shown in Figs. 2 and 3. Given that the region of interest is an urban area, where LULC information is crucial (Lin et al., 2016), we used the multilayer BEP-BEM scheme to represent the urban zones (Martilli et al., 2002; Salamanca et al., 2010). The BEP parameterization considers the interaction between buildings and the atmospheric boundary layer, including the effects of vertical and horizontal motion, Turbulent Kinetic Energy (TKE), and thermal stability. Additionally, it is coupled with the BEM parameterization, which considers the energy produced inside buildings, including variables related to air-

Table 2
Air-quality monitoring stations of the Madrid city network with their coordinates. The value of their urban fraction (F_{urb}) and LCZ in 1970 and 2020 is shown.

STATION	LONGITUDE (°)	LATITUDE (°)	F_{urb}		LCZ	
			1970	2020	1970	2020
1. Escuelas Aguirre	−3.682	40.421	0.86	0.96	LCZ 2	LCZ 2
2. Farolillo	−3.732	40.394	0.76	0.88	LCZ 5	LCZ 2
3. Plaza del Carmen	−3.703	40.419	1	1	LCZ 2	LCZ 2
4. Cuatro Caminos	−3.707	40.445	0.83	0.98	LCZ 5	LCZ 2
5. Ensanche de Vallecas	−3.612	40.372	0.22	0.81	LCZ 6	LCZ 5
6. Plaza Elíptica	−3.718	40.385	0.95	0.97	LCZ 5	LCZ 5
7. JMD Centro	−3.711	40.416	0.83	0.87	LCZ 5	LCZ 5
8. Moratalaz	−3.645	40.407	0.73	0.97	LCZ 5	LCZ 5
9. Juan Carlos I	−3.609	40.465	0	0	LCZ B	LCZ B

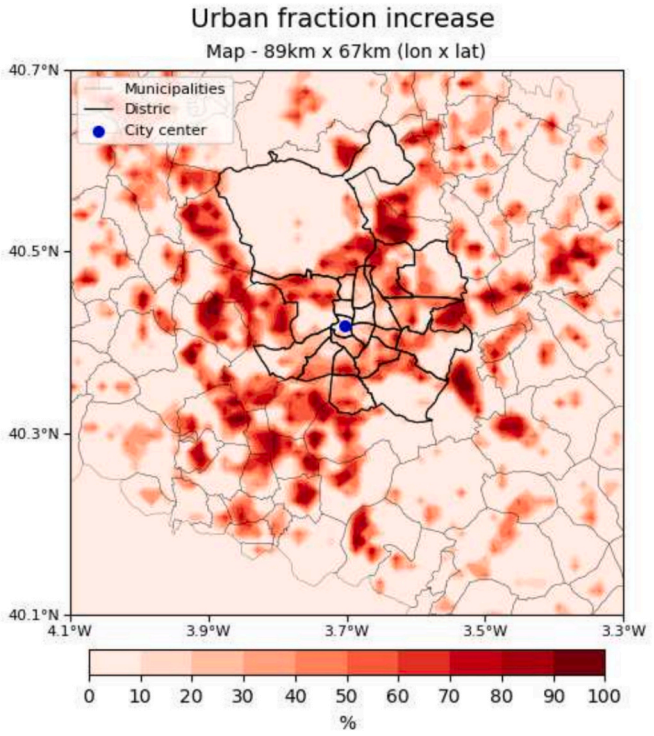

Fig. 2. Difference in urban fraction (%) in the Madrid region from 1970 to 2020. The black lines indicate the different districts of the city of Madrid, and the city center is marked by a blue dot. (For interpretation of the references to colour in this figure legend, the reader is referred to the web version of this article.)

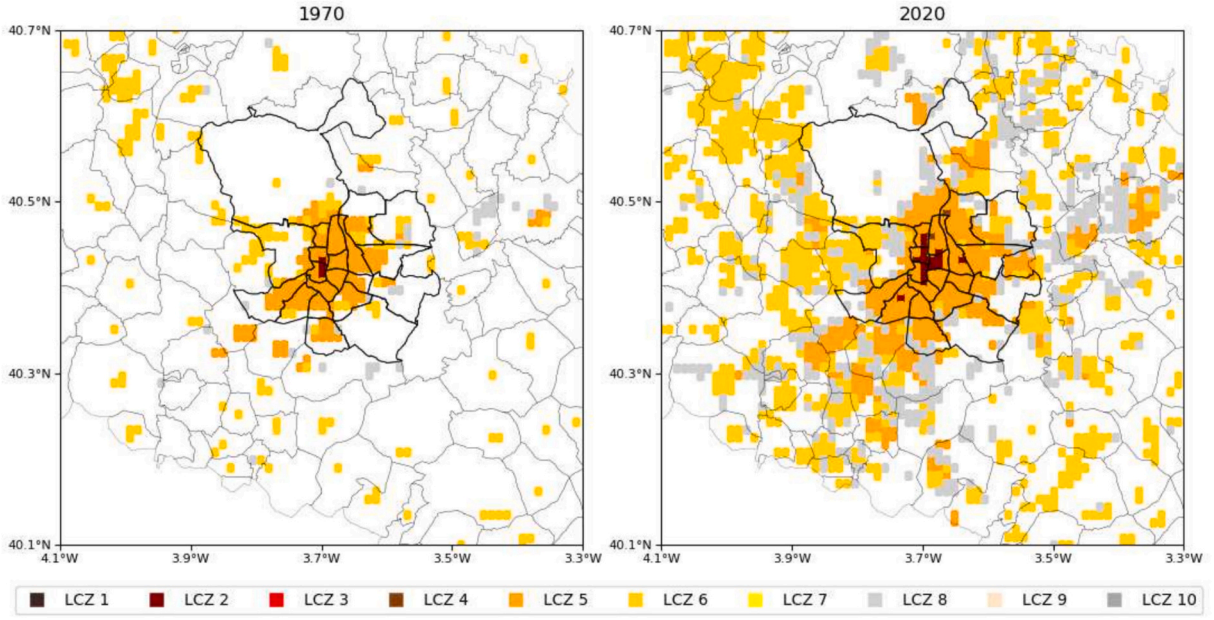

Fig. 3. Map of urban LCZs over Madrid for 1970 and 2020. The majority urbanized landscape (LCZ types 1 to 10) is classified as Compact Mid-rise (LCZ 2), Compact Low-rise (LCZ 3), Open High-rise (LCZ 4), Open Mid-rise (LCZ 5), Open Low-rise (LCZ 6), Large Low-rise (LCZ 8) and Sparsely Built (LCZ 9). There were no areas classified as Compact High-Rise (LCZ 1), Lightweight Low-Rise (LCZ 7) and Heavy Industry (LCZ 10).

conditioning or heating systems. Since our objective is to isolate the effect of urban development, we have conducted simulations without considering the impact of air conditioning. However, for model validation, the air conditioning parameterization has been activated. The validation is against data obtain in 2020, when the air conditioning is already largely used in the city. Previous studies have shown that this parameterization can accurately estimate this energy at the city scale if morphological parameters and building thermal properties are correctly specified (Salamanca et al., 2013; Tewari et al., 2017).

Fig. 3 illustrates the graphical representation of the different types of urban morphology present in the city of Madrid in 1970 and 2020. Each grid point has been classified in a LCZ based on the urban parameters calculated previously, in agreement with the ranges defined by Stewart and Oke (2012) (detailed classification can be found in Appendix A.2 of the supplemental material.). This classification is only performed for representation purposes, but are not used in the simulation since the urban morphology is given at each grid point, and the building thermal and optical properties are the same for all the buildings.

2.4. Urban development data

We used cadastral data with rich thematic property attribution, such as construction year, to assess the potential effects of Madrid's current and historical settlement over the last 50 years (1970–2020). A procedure similar to the one described in Uhl et al. (2023) has been followed. We scraped and processed Cadastral building footprint data using INSPIRE information via the ATOM interface for the autonomous region of Madrid (last accessed on October 1st, 2021). We stratified the building records by their construction year into temporal epochs based on 5-year intervals between 1970 and 2020. A Digital Model of Building Surfaces with 2.5 m resolution (MDSnE2.5, based on LiDAR coverage 2009–2015) from the Spanish National Geographic Institute was employed to extract the average building heights for each footprint. The recent coverage of the MDS implies that we assume a constant height, in addition to the current height being that of the historical building footprints. For the model setup, we estimated spatial aggregation into grid cells within regular spatial grids of 100 m $\times$ 100 m by calculating the building footprint area and fraction, building contour, lambda (sum of heights and vertical building area), and average building heights.

2.5. Analysis of the surface energy balance in the simulations

Micrometeorology in urban areas is quite different than in rural areas. This has been confirmed and extensively investigated by Rotach (1993), where turbulent variables were measured at different heights within and above a street canyon. He found that turbulent flows are not constant with height in the lower part of the Urban Roughness Sublayer (URS, 1–3 times the mean building height). Consequently, the Monin-Obukhov Similarity Theory cannot be applied in urban areas since the invariance with height of turbulent flows is not met. Therefore, urban surface roughness determines the turbulent characteristics of the urban environment, and the fact that a city is composed of buildings of variable size must be taken into account since this particularity significantly affects the structure of the UBL developed, where the two most important factors are:

- **Mechanical**: Buildings create a drag effect that leads to a loss of momentum. Additionally, they promote the transfer of energy from larger to smaller eddies.
- **Thermal**: Buildings induce differential heating/cooling of sunlit/shaded surfaces within the urban landscape. This differential heating results in the trapping of radiation within street canyons. Furthermore, buildings and roads (being impervious) reduce latent heat fluxes, which, in turn, affect the sensible heat flux released into the atmosphere.

These factors show that the impact of urbanization goes beyond temperature, as urbanization also affects wind patterns and the characteristics of the Urban Canopy Layer (UCL). In general, the wind field in the UCL is more complex than in rural areas and is strongly influenced by the details of the building morphology (Louka et al., 2000; Oke et al., 2017). Due to this mechanical effect, wind speed tends to decrease as air moves into urban areas (Zhu et al., 2016) or as urbanization increases (Hou et al., 2013). However, urban areas often have higher temperatures during night-time than rural areas, which can induce direct thermal circulation. Observational evidence of both mechanical and thermal effects on winds in urban areas are provided in Bornstein and Johnson (1977).

The study of the SEB of urban surfaces during different meteorological periods can lead to a better understanding of the factors that mitigate or amplify urban temperatures anomalies. In the case of the model used in this study, the SEB is described by the following equation:

$$Q^* = Q_H + Q_E + \Delta Q_S \tag{1}$$

where Q^* is the net radiation, Q_H is the sensible heat flux, Q_E is the latent heat flux, and ΔQ_S is the storage heat flux. The sign criterion used in this paper is that Q^* and ΔQ_S are defined as positive when it is directed towards the surface and negative when directed outwards from the surface. On the contrary, the heat fluxes Q_H and Q_E are defined positive when they are outgoing from the surface.

3. Results

3.1. Model validation

In order to evaluate the 2-m air temperature (T_2) results obtained in the WRF simulations, data from different meteorological

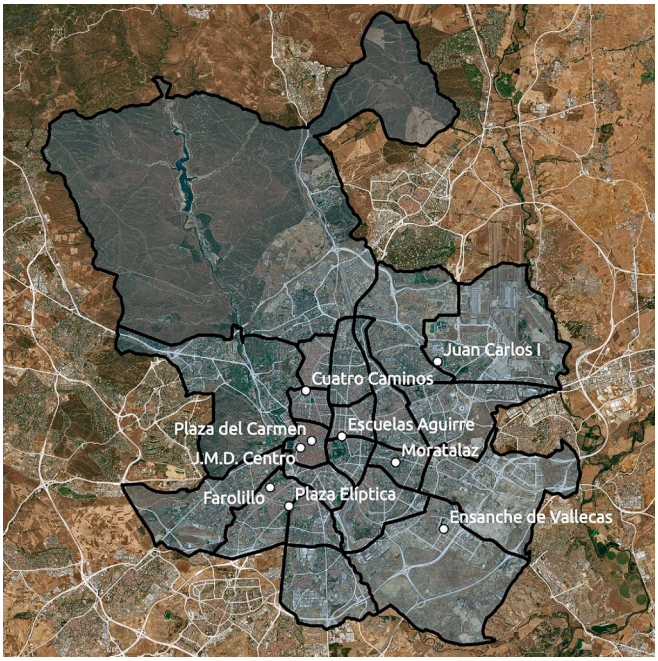

Fig. 4. Location and name of air-quality monitoring stations of the Madrid city network used for the study-validation.

stations belonging to the air quality monitoring stations of the Madrid city network were used (Data Air Quality Network, see Fig. 4). Hourly data were used for both periods and in Table 2 detailed information regarding the location of each station, the urban fraction of the area, as well as the LCZ based on the categories defined by Stewart and Oke (2012).

The statistical parameters Mean Bias Error (MBE) and Root Mean Square Error (RMSE) are used to quantify the model's accuracy:

$$\mathrm{MBE} = \frac{1}{N}\sum_{i=1}^{N}(A_i - O_i) \tag{2}$$

$$\mathrm{RMSE} = \sqrt{\frac{1}{N}\sum_{i=1}^{N}(A_i - O_i)^2} \tag{3}$$

where N is the total number of temperature data points, A_i it refers to the data simulated by the WRF model and O_i to the observed data.

The model underestimates the values of daytime temperature at all stations except one during the winter period (Table 3). Additionally, the model tends to capture nighttime temperatures more accurately, as reflected in lower MBE and RMSE values during this period. On the contrary, during the summer period the model tends to overestimate the values of daytime temperatures at five out of the nine stations, with MBE values less than 0.5 °C (Table 4). In this case, the model tends to overestimate daytime temperatures and underestimate nighttime temperatures, with lower MBE and RMSE values compared to the winter period.

We can conclude that the results for the summer period are good both during the daytime and at nighttime. In the case of the winter period, there is an underestimation during daytime, but these results are acceptable given the difficulty of simulating a period of stable atmospheric conditions.

3.2. *Impact of urban expansion on the near-surface air temperature*

In this section, we analyze and quantify the near-surface air temperature increase due to the urban development in the city of Madrid and surroundings. To do this, we use the model variable of air temperature at the lowest model level (T_a). The top of the lowest model level is at 5 m above the surface and its mass center is around 2.5 m above ground level. In our analysis, to be consistent, we use T_a because the standard T_2 output from the WRF model, in rural areas, results from a logarithmic interpolation modified to account for atmospheric stability, based on Monin-Obukhov Similarity Theory (MOST). However, in urban areas, where MOST is not valid, T_2 is simply the temperature of the lowest model level (when BEP-BEM is used).

In the study area, there are no pixels where the urban fraction decreased in 2020 compared to 1970, but there are pixels where it remained the same. In these pixels, the average increase in T_a is negligible during the day and only 0.3 °C during the night for both periods, indicating that the increase of urbanization of the surrounding areas affect also the regions that were already urban in 1970. This can be observed in Fig. 5, which shows the spatial differences of the T_a between 2020 and 1970 for day, nighttime and for both

Table 3
Model evaluation results for the winter period.

STATION	ALL DAY		DAYTIME (08-17 UTC)		NIGHTTIME 19-06 UTC)	
	MBE (°C)	RMSE (°C)	MBE (°C)	RMSE (°C)	MBE (°C)	RMSE (°C)
Escuelas Aguirre	−1.62	2.26	−2.72	3.14	−0.62	0.88
Farolillo	−0.73	1.85	−1.89	2.26	0.21	1.31
Plaza del Carmen	−1.33	2.18	−2.08	2.85	−0.68	1.37
Cuatro Caminos	−1.57	2.23	−2.40	2.88	−0.70	1.04
Ensanche de Vallecas	−0.67	1.39	−1.54	1.76	0.21	0.49
Plaza Elíptica	−0.53	1.77	−1.78	2.26	0.55	1.13
JMD Centro	−2.10	2.26	−2.54	2.67	−1.69	1.79
Moratalaz	0.17	1.06	0.14	1.32	0.33	0.64
Juan Carlos I	−1.80	2.01	−1.83	2.01	−1.64	1.81
MEAN VALUE	−0.93	1.89	−1.85	2.35	−0.45	1.16

Table 4
Model evaluation results for the summer period.

STATION	ALL DAY		DAYTIME (06–18 UTC)		NIGHTTIME (20–04 UTC)	
	MBE (°C)	RMSE (°C)	MBE (°C)	RMSE (°C)	MBE (°C)	RMSE (°C)
Escuelas Aguirre	0.40	1.45	0.41	1.62	0.54	1.32
Farolillo	−0.10	1.16	0.25	1.36	−0.46	0.84
Plaza del Carmen	0.31	0.88	0.31	0.95	0.35	0.85
Cuatro Caminos	0.09	1.34	0.56	1.55	−0.29	0.98
Ensanche de Vallecas	−0.45	1.25	0.13	1.21	−1.06	1.22
Plaza Elíptica	0.43	1.18	0.17	1.14	0.89	1.34
JMD Centro	0.01	1.12	0.35	1.29	−0.27	0.85
Moratalaz	0.32	1.52	0.69	1.70	0.01	1.33
Juan Carlos I	−0.82	1.81	−0.41	1.21	−1.09	2.29
MEAN VALUE	0.02	1.30	0.27	1.34	−0.15	1.22

periods. The city center pixels (which do not change their urban fraction) experience this weak nocturnal increase in T_a due to the expansion of surrounding urban areas that contribute to the city temperature increase. During the summer period, the average temperature increases 0.25 °C during the day and approximately 1.5 °C at night in areas that have undergone urban development (those pixels of 1 km^2 where urban fraction has increased). In specific locations, the maximum differences are around 1.5 °C during the day and up to 7 °C at night, due to factors related to wind direction and the city's urban expansion configuration. In the winter period, the average temperature rise is 0.4 °C during the day and 1.5 °C at night. Maximum anomalies of approximately 2 °C during the day and around 6.5 °C at night are observed in certain areas, as seen in the summer period. The smaller temperature differences at night during the winter period compared to the summer one, are likely attributed to typical thermally-driven flows that occur overnight under stable conditions (Fernández García et al., 1996; Román-Cascón et al., 2019) in the area of Madrid.

The temperature anomalies are more pronounced at night since the city expansion reduces the rate of cooling during the late afternoon and night, resulting in higher minimum temperatures in heavily urbanized areas. The materials used in urban construction are characterized by their enhanced heat capacity and, as a result, higher thermal inertia. This leads to significant heat storage that increases the energy available to maintain a positive sensible heat flux during night and contributes to the typically warmer nighttime air temperatures. In addition, the low PBL height during night makes that a small change in the sensibile heat flux to the atmosphere has a large impact on air temperatures., compared to the daytime situation when the heat is mixed over a much thicker layer.

The percentage of pixels where diurnal temperature shows an increase of more than 0.25 °C due to urban development accounts for 45 % of urban pixels in 2020 (urban fraction greater than 50 %) for the summer period, while this impact extends to 88 % during the night. In contrast, during the stable winter period, we find that during the day, the affected area is 51 %, and during the night, is 81 %. We can conclude that the area in which the near-surface air temperatures increase due to the urbanization of Madrid is greater during the night than during the day. When we compare both periods, the results show a greater area with significant increase in temperature during the day in the winter period (6 % more than in summer), but a greater expansion during the night in the summer period (7 % more than in winter). To understand these differences, we extend the analysis to the energy balance of the urban surfaces during these contrasting conditions since this can lead to a better understanding of the factors that mitigate or amplify the intensity and extent of the urban heat (Section 3.3).

Both the intensity and expansion of Madrid's UHI are greater at night than day. To understand its cause, we analyze the trend in nighttime temperatures due to the urban growth of Madrid over the past 50 years, as depicted in Fig. 6. This figure shows the change in nighttime temperature versus the increase in urban fraction but only for those areas (1 km^2 pixels) located at an altitude between 600 and 700 m above sea level, to account for changes not related to altitude. The method for this analysis involves grouping these pixels in increments of 10 % of the urban fraction for the 1970–2020 period. This means that the first group consists of all pixels that have increased their urban fraction between 1 % and 10 %, the second group for pixels with an increase between 11 and 20 %, and so on, up to the last group, which includes those with an increase between 91 and 100 %. The linear regression of the median values of these

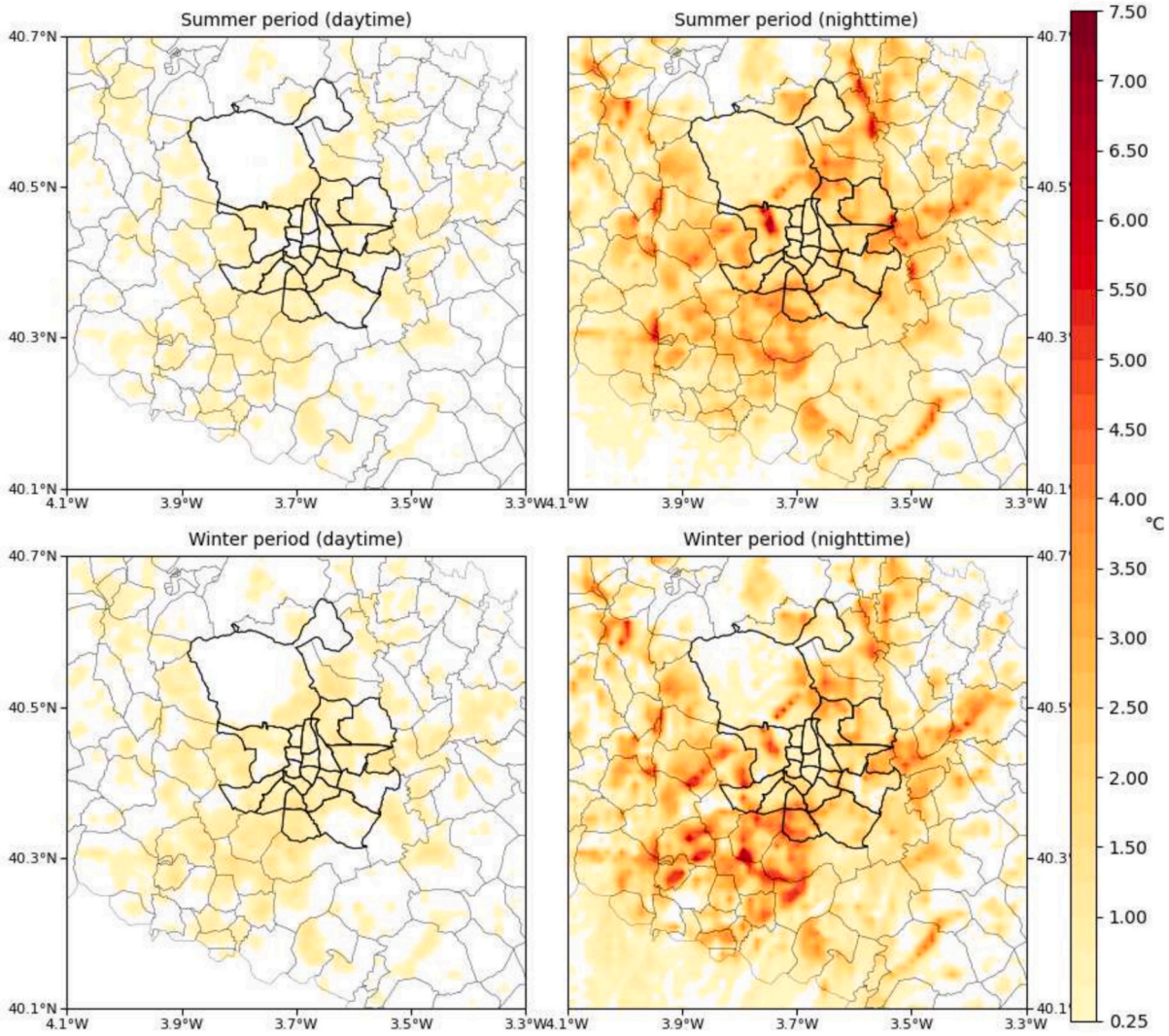

Fig. 5. Increase in the daily mean T_a due to urban development (1970–2020) in the simulated summer (above) and winter (below) periods during daytime (left) and nighttime (right) hours.

groups shows a trend of increase in nighttime temperature. Specifically, a 10 % growth in urban fraction leads to an increase in nighttime temperatures by 0.225 °C in the summer period and 0.249 °C in the winter period. It's worth noting the significant variability observed, as an increase in the urban fraction in a specific area also depends on the configuration of this urban development. Therefore, urban development clearly tends to increase nighttime temperatures, but it is difficult to precisely determine this increase because it depends on many characteristics of the city's configuration that are challenging to quantify.

The best correlation is for the summer period because the higher solar radiation absorption of urban surfaces amplifies the intensity, duration, and frequency of heatwaves. Studies in Europe have identified a significant contribution of urbanization to increasing trends in extreme temperature indices (Lauwaet et al., 2016; Ma et al., 2024). Furthermore, the response of the UHI to extreme heat episodes has been modeled in many studies. In general, simulated values during a heatwave intensified, mainly due to lower humidity and reduced wind speed in urban areas during the heatwave. The intensity monitored at night was significantly higher, validating its typical nighttime dominance (Li and Bou-Zeid, 2013; Zhao et al., 2018; Ao et al., 2019; He et al., 2020).

3.3. Analysis of the surface energy balance

Urban areas are highly impermeable and present less vegetation than rural, which reduces moisture storage in the subsurface and causes the available energy to be used as surface heating instead of producing evaporation (Wang et al., 2012). To represent each term of the SEB in our study, we consider the urban grids with an urban fraction change from 1970 to 2020 (only pixels with altitude between 600 and 700 m are used). A decrease in Q_E is observed (Figs. 7 and 8), which is more pronounced during the winter period

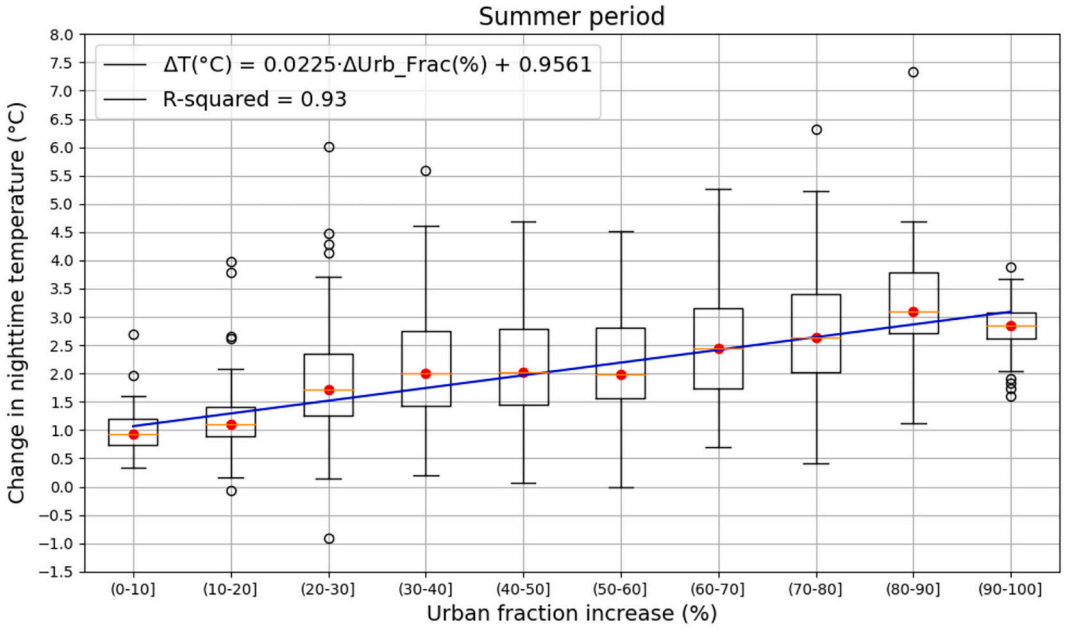

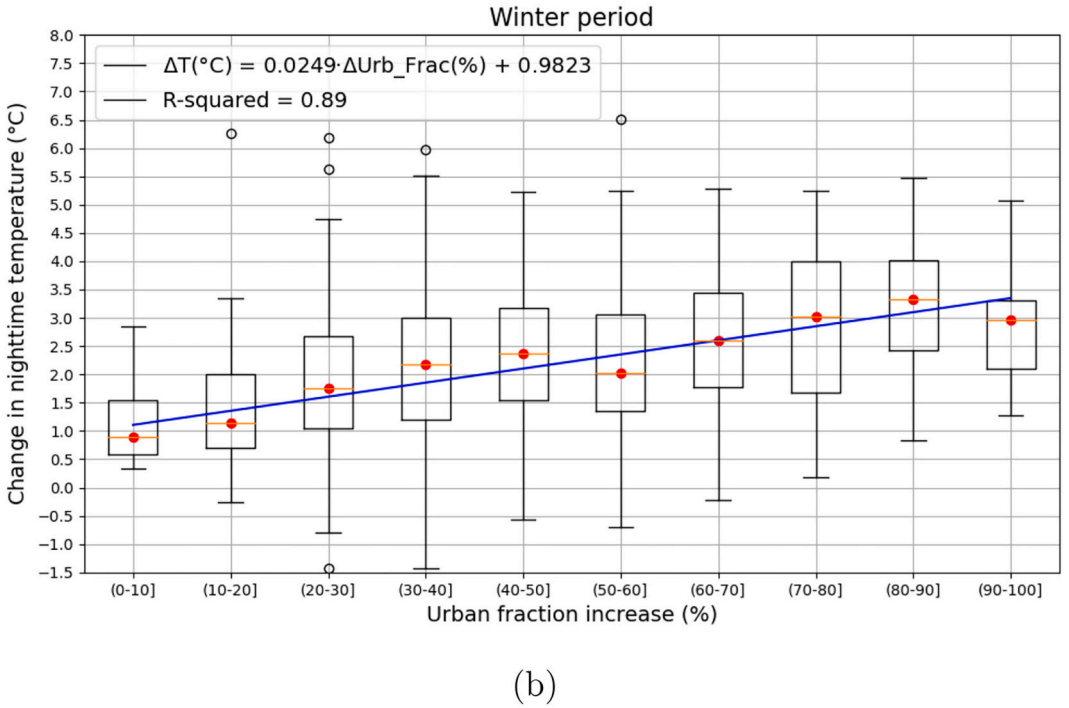

Fig. 6. Boxplots of the increase in night-time T_a (average over the period) according to the increase in urban fraction: (a) summer period and (b) winter period.

(wetter season) and almost negligible during the summer period (drier season). This difference in moisture between the two periods leads to important changes in SEB.

In the winter period, the daytime decrease in Q_E in 2020 compared to the 1970 values (Fig. 7) is compensated by an increase in ΔQ_S during the daytime in 2020 (approximately 30 % during the midday hours), rather than an increase of Q_H that stays relatively

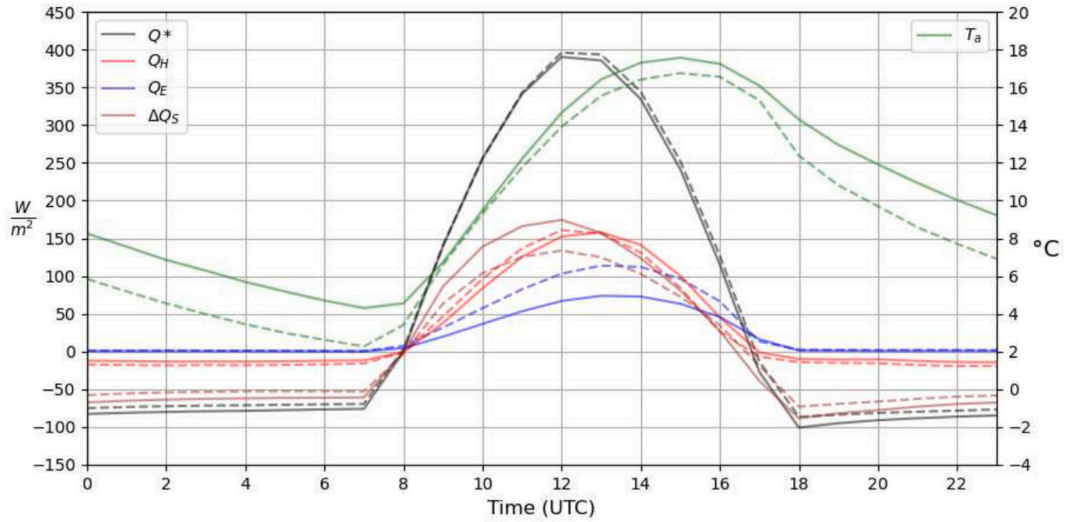

Fig. 7. Surface energy balance and T_a (green lines) for the winter period (dashed lines for 1970 and solid lines for 2020). These averages are calculated over all the days of the period and represent the points that have experienced an increase in their urban fraction between 1970 and 2020, situated at an altitude between 600 and 700 m.a.s.l. (For interpretation of the references to colour in this figure legend, the reader is referred to the web version of this article.)

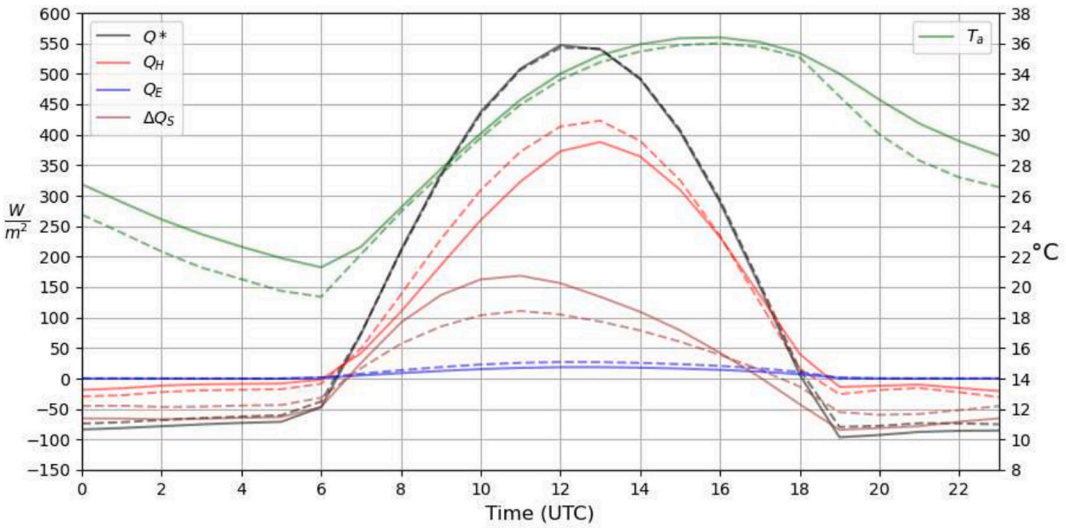

Fig. 8. Surface energy balance and T_a (green lines) for the summer period (dashed lines for 1970 and solid lines for 2020). These averages are calculated over all the days of the period and represent the points that have experienced an increase in their urban fraction between 1970 and 2020, situated at an altitude between 600 and 700 m.a.s.l. (For interpretation of the references to colour in this figure legend, the reader is referred to the web version of this article.)

unchanged, with only a shift in the maximum towards the afternoon hours in 2020 compared to 1970. This is attributed to the greater solar radiation absorption through multiple reflections, and a larger surface area for this storage. On the other hand, during the nighttime the more negative ΔQ_S values in 2020 (directed towards the atmosphere) release energy into the atmosphere creating a small increase in the Q_H (slightly less negative). This phenomenon leads to much stronger impact on the near-surface air temperature at night compared with that during the day because the stable stratification during the night decreases the turbulent mixing between near surface and above layers related to what happen during the day with unstable stratification (Bohnenstengel et al., 2011; Wouters et al., 2013).

In the summer period (Fig. 8), the daytime Q_H decreases from 1970 to 2020 due to the mechanical interaction effect caused by the city's roughness, and the increased thermal inertia. However, the daytime near surface air temperature slightly increased in 2020 compared to 1970. The greater number of buildings reduces average wind speed and heat loss by decreasing turbulence in the UCL. Despite an increase in the vertical temperature gradient, the Q_H decreases because the mechanical effect dominates over the thermal

effect. Again, the increased thermal inertia and the decrease in turbulence heat transport in the UCL during the day lead to an increase in the storage term. This increase in the ΔQ_S (approximately 50 % during the midday hours) during the day is released back into the atmosphere at night (in both periods), increasing the city air temperature and exacerbating the UHI effect, both in intensity and extent. Grimmond and Oke (1999) studied the heat storage flux for seven cities in North America, concluding that it is an important component of the energy balance in all the urban studied sites (representing between 17 % and 58 % of the daytime net radiation).

In order to understand the Q_H decrease in the summer period in 2020 compared to 1970 we analyze the modifications observed in the vertical profiles of potential temperature and TKE, one of the most studied turbulent parameters (Arya, 2001), which is generated by both wind shear and buoyancy forces. The TKE budget in the UCL is complicated by multiple generation and dissipation mechanisms, as well as TKE redistribution and transport due to spatial inhomogeneities (Fernando, 2010). The most common hypothesis in the study of urban areas is that these zones are usually characterized by increased roughness and Q_H compared to the rural areas that they replace, leading generally to higher TKE. This results in greater mixing within the boundary layer and increased entrainment. However, while this may be true for the whole PBL, it may not in the lower part of the UCL. Rotach (1993), for example, measured that the peak of TKE is in general in the upper part of the roughness sublayer, well above roof tops, and that the TKE decreases in the lowest part of the canopy. This is in agreement with CFD simulations (Santiago et al., 2007). In our case, we observed reduction in Q_H in the summer simulation when using land cover and land use data from 2020 compared to 1970. As mentioned earlier several mechanisms are at play: the increase of thermal inertia, the creation of TKE generated by the increased shear induced by building roughness, the decrease of TKE in the UCL, along with many other factors related to wind direction and city characteristic's, which are challenging to quantify.

Focusing on areas that have experienced an increase in their urban fraction from 1970 to 2020, as illustrated in Fig. 9, we observe that, on average, over the five simulated days (at 13 UTC, which corresponds to the time of maximum Q_H), these areas exhibit a higher potential temperature near the surface (within the UCL) in the 2020 simulation compared to the 1970 simulation, during both summer and winter periods. However, outside the UCL (from 50 m above the ground), we observe the opposite effect, but only during the summer period. This results in a stronger vertical temperature gradient in the 2020 simulation due to urban development. Additionally, the increased number of buildings reduces average wind speeds and heat loss by decreasing TKE in the UCL (Fig. 10), and these differences are more pronounced during the summer period (again on average for the five days simulated at 13 UTC which is the time of maximum Q_H). Therefore, this decrease in Q_H during the summer period is due to reduced vertical mixing in the layers closer to the ground, causing more heat to accumulate in the UCL.

This decrease in vertical mixing shown above, due to a reduction in turbulence in the UCL, raises questions about whether the model is accurately quantifying these mechanisms, as we lack observational data on turbulent parameters in the city of Madrid to validate these simulations. This is, in part, due to the challenges associated with calculating reliable turbulent parameters from observational measurements in complex urban environments. Most observations consist of traditional surface-level measurements without vertical profiles (particularly useful in areas with tall or significantly variable building heights) and often include only a few common meteorological variables (e.g., temperature, wind, precipitation, and humidity). A comprehensive set of complementary observations, including turbulent fluxes, is often absent. Consequently, the lack of these observations complicates the understanding of these interactions and feedback mechanisms.

Given the challenges associated with obtaining accurate and representative measurements of wind and turbulence in intricate urban environments, the investigation conducted by Román-Cascón et al. (2023) aims to explore distinctions when utilizing data from sonic anemometers deployed at different emplacements: street and terrace. Throughout their study, they have discerned that the recorded values of turbulence parameters (TKE, u*, and Q_H) and wind speed, as obtained from the sonic anemometers, are notably lower for the device situated on the street when compared with its counterpart on the terrace (positioned at a height of 26 m above street level). Notably, these findings align coherently with the outcomes derived from our model. These complementary observations are crucial for future urban management plans and for designing more appropriate strategies to mitigate the urban growth effect. In this sense, more-intense field campaigns with a larger number of sonic anemometers would be necessary to further explore the microscale differences among the different parts in the city (both vertical and horizontal). Therefore, this should serve as an incentive to conduct measurement campaigns in the future to determine whether the model results explain the factors that amplify urban temperature anomalies.

4. Summary and conclusions

This work presents the impact of the urban expansion in Madrid on the local atmospheric conditions for two periods in different seasons: an intense heatwave event (August 2020) and a strongly stable period in winter (February 2020). In order to assess the impact of the exceptional of Madrid's urban growth over the last 50 years (1970–2020), we conducted paired simulations with identical meteorology for each period driven by two LULC scenarios in 1970 and 2020. These databases (Uhl et al., 2023) include urban parameters such as urban fraction and mean building height. This provides a realistic view of LULC for these decades, and it allows us to parameterize urban development. The main outcomes are summarised below:

- One of the most significant findings of this study is the influence of urban expansion on near-surface air temperatures. This impact is more pronounced at night for both simulated periods, as it reduces the rate of cooling during the late afternoon and night, resulting in higher minimum temperatures in heavily urbanized areas. The percentage of urban pixels in 2020 (urban fraction greater than 50 %) showing an increase in nighttime near-surface air temperatures of more than 0.25 °C due to urban development is 88 % during the intense heatwave event and 81 % during the period with stable winter conditions. The average impact of the increase is

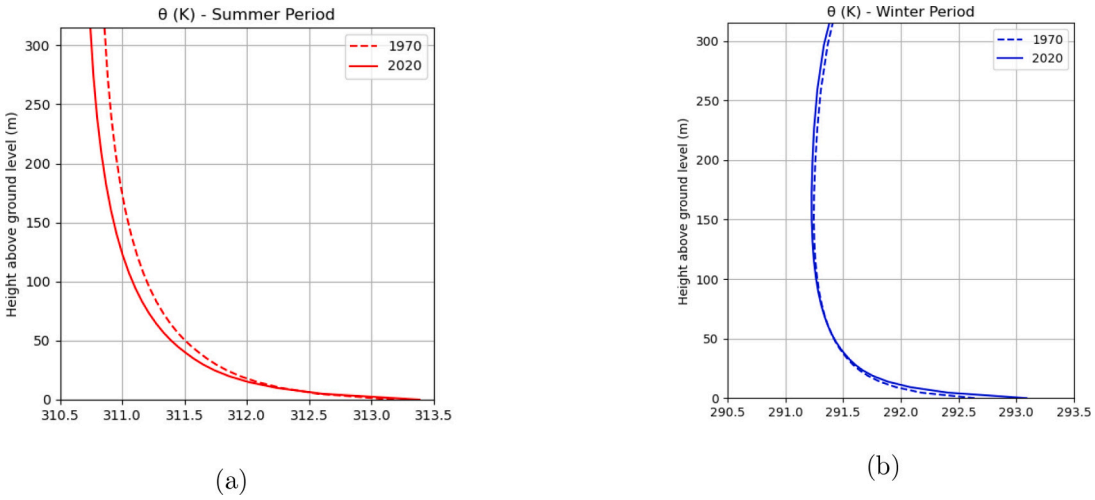

Fig. 9. Vertical profiles of potential temperature on average for the five days simulated (at 13 UTC wich is the time of maximum Q_H). These are the averages of the points that have increased their urban fraction between 1970 and 2020 and are located at an altitude between 600 and 700 m.

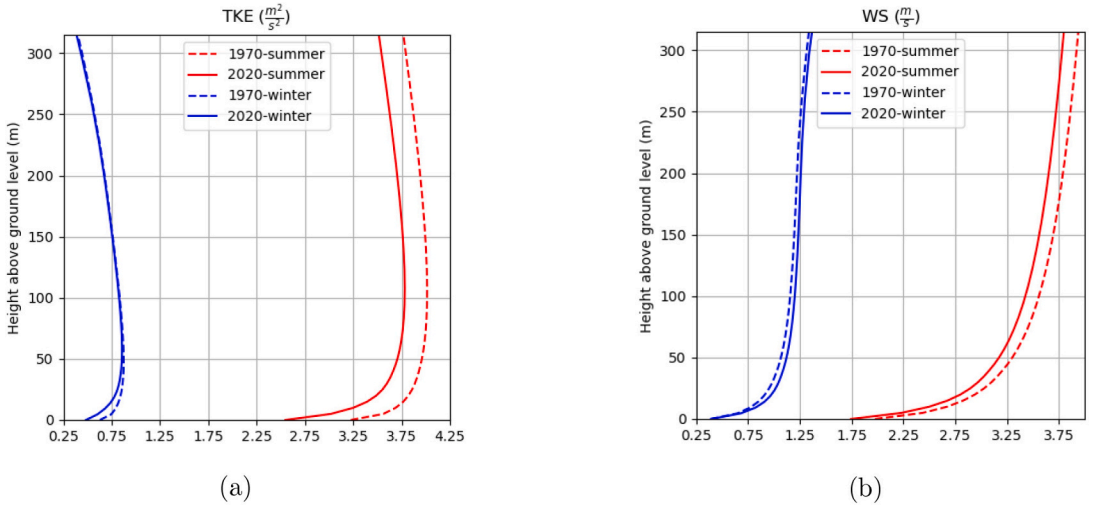

Fig. 10. Vertical profiles of turbulent kinetic energy (TKE) and wind speed (WS) on average for the five days simulated (at 13 UTC wich is the time of maximum Q_H), respectively. These are the averages of the points that have increased their urban fraction between 1970 and 2020 and are located at an altitude between 600 and 700 m.

1.5 °C for both simulated periods. However, specific areas with substantial urban development exhibit a higher impact, reaching up to 7 °C during the summer period and 6.5 °C during the winter period for the nighttime near-surface air temperatures.

- The trend of urban growth is to increase nighttime temperatures near the surface for both simulated periods. Specifically, a 10 % growth in urban fraction leads to an increase in nighttime temperatures by 0.225 °C in the intense heatwave event and 0.249 °C in the period with stable winter conditions. The characteristics of urban surfaces, including material properties and city morphology, contribute significantly to this nighttime temperature effect.
- Urbanization has a significant influence on the surface energy balance terms. There is a decrease in Q_E because urban areas are highly impermeable and have less vegetation, which reduces moisture storage in the subsurface and directs available energy towards surface heating instead of producing evaporation. This reduction in Q_E is more pronounced during the winter period (wetter season) and almost negligible during the summer period (drier season). During the winter period, daytime Q_H values remain approximately the same but shift their peak towards the afternoon hours. On the other hand, in the summer period, daytime Q_H decreases due to the mechanical interaction effect caused by the city's roughness. Furthermore, the high heat capacity of urban surfaces with numerous buildings increases the ΔQ_S during the daytime. This is attributed to the greater solar radiation absorption through multiple reflections, and a larger surface area for this storage. This increase in the ΔQ_S during the day is released back into

the atmosphere at night in both periods, exacerbating the increase in nighttime near-surface air temperatures, both in intensity and extent.

The decrease in Q_H during the summer period is due to reduced vertical mixing in the layers closer to the ground, causing more heat to accumulate in the UCL. The mechanical interaction effect caused by the city's roughness reduces average wind speeds and heat loss by decreasing turbulence in the UCL. Despite an increase in the vertical temperature gradient, the Q_H decreases because the mechanical effect dominates over the thermal effect. This decrease in vertical mixing, due to a reduction in turbulence in the UCL, raises questions about whether the model is accurately quantifying these mechanisms, as we lack observational data on turbulent parameters in the city of Madrid to validate these simulations. In this sense, more-intense field campaigns with a larger number of sonic anemometers would be necessary to further explore the microscale differences among the different parts in the city (both vertical and horizontal). Therefore, this should serve as an incentive to conduct measurement campaigns in the future to determine whether the model results explain the factors that amplify urban temperature anomalies. Additionally, it would be interesting to consider the role played by both the city breeze and the mountain-valley breeze. The interactions between UHI-induced urban flows (Catalano et al., 2012) and mesoscale circulations, such as mountain-valley and land-sea or lake breezes, are the subject of active research (Miao et al., 2015; Ganbat et al., 2015; Yu et al., 2021) and may be more significant influences on microclimate than land cover and surface properties (Martilli et al., 2020). Finally we stress that this study neglects the warming induced by climate change. Investigating the relative impact of urban expansion and climate change as well as the interactions will be a subject of future studies.

CRediT authorship contribution statement

J. Carbone: Writing – original draft, Visualization, Validation, Supervision, Software, Resources, Methodology, Investigation, Formal analysis, Data curation, Conceptualization. **B. Sanchez:** Writing – review & editing, Supervision, Software, Resources, Methodology, Investigation, Formal analysis, Data curation, Conceptualization. **C. Román-Cascón:** Writing – review & editing, Supervision, Methodology, Investigation, Formal analysis, Data curation, Conceptualization. **A. Martilli:** Writing – review & editing, Supervision, Software, Methodology, Investigation, Formal analysis, Data curation. **D. Royé:** Writing – review & editing, Supervision, Resources, Investigation, Formal analysis, Data curation. **C. Yagüe:** Writing – review & editing, Supervision, Project administration, Methodology, Investigation, Funding acquisition, Formal analysis, Data curation, Conceptualization.

Declaration of competing interest

The authors declare that they have no known competing financial interests or personal relationships that could have appeared to influence the work reported in this paper.

Acknowledgements

This work has been funded by the Madrid Autonomous Community and the European Commission (FSE) under the AIRTEC-CM (S2018/EMT4329) project, as well as in the framework of the I + D + i Spanish National Projects PID2023-149246OB-C21 project (MULTIURBAN-I) and PID2023-149246OB-C22 project (MULTIURBAN-II), funded by the Ministerio de Ciencia e Innovación of Spain MCIN/AEI/10.13039/ 501100011033/ FEDER, UE. The Madrid City Council is specially acknowledged for its support for the data provided of the air-quality monitoring stations.

Appendix A. Supplementary data

Supplementary data to this article can be found online at https://doi.org/10.1016/j.uclim.2024.102198.

Data availability

Data will be made available on request.

References

AEMET, 2022. Olas de calor en España desde 1975. https://www.aemet.es/documentos/es/conocermas/recursos_en_linea/publicaciones_y_estudios/estudios/Olas_calor/Olas_Calor_Actualizacion_Junio_2019.pdf.

Ao, X., Wang, L., Zhi, X., Gu, W., Yang, H., Li, D., 2019. Observed synergies between urban heat islands and heat waves and their controlling factors in Shanghai, China. J. Appl. Meteorol. Climatol. 58, 1955–1972. https://journals.ametsoc.org/view/journals/apme/58/9/jamc-d-19-0073.1.xml. https://doi.org/10.1175/JAMC-D-19-0073.1.

AR6 - IPCC, 2022. Climate Change 2022 – Impacts, Adaptation and Vulnerability: Working Group II Contribution to the Sixth Assessment Report of the Intergovernmental Panel on Climate Change. Cambridge University Press. https://doi.org/10.1017/9781009325844.

Arnfield, A.J., 2003. Two decades of urban climate research: a review of turbulence, exchanges of energy and water, and the urban heat island. Int. J. Climatol. 23, 1–26. https://doi.org/10.1002/joc.859.

Arya, P.S., 2001. Introduction to Micrometeorology. Elsevier.

Barriopedro, D., García-Herrera, R., Ordóñez, C., Miralles, D.G., Salcedo-Sanz, S., 2023. Heat waves: physical understanding and scientific challenges. Rev. Geophys. 61. https://doi.org/10.1029/2022rg000780.
Bohnenstengel, S.I., Evans, S., Clark, P.A., Belcher, S., 2011. Simulations of the London urban heat island. Q. J. R. Meteorol. Soc. 137, 1625–1640. https://doi.org/10.1002/qj.855 arXiv:https://rmets.onlinelibrary.wiley.com/doi/pdf/10.1002/qj.855.
Bornstein, R.D., Johnson, D.S., 1977. Urban-rural wind velocity differences. Atmos. Environ. 11, 597–604 (1967). https://www.sciencedirect.com/science/article/pii/0004698177901123. https://doi.org/10.1016/0004-6981(77)90112-3.
Bougeault, P., Lacarrere, P., 1989. Parameterization of orography-induced turbulence in a mesobeta–scale model. Mon. Weather Rev. 117, 1872–1890. https://journals.ametsoc.org/view/journals/mwre/117/8/1520-0493_1989_117_1872_pooiti_2_0_co_2.xml, 10.1175/1520-0493(1989)117<1872:POOITI>2.0.CO;2.
Catalano, F., Cenedese, A., Falasca, S., Moroni, M., 2012. Numerical and Experimental Simulations of Local Winds, National Security and Human Health Implications of Climate Change. NATO Science for Peace and Security Series C: Environmental Security. Springer, Dordrecht, pp. 199–218. https://doi.org/10.1007/978-94-007-2430-3_17.
Chapman, R., Howden-Chapman, P., Whitwell, K., Thomas, A., 2017. Towards zero carbon? Constrained policy action in two New Zealand cities. Aust. J. Environ. Manag. 24, 97–116. https://doi.org/10.1080/14486563.2017.1309696.
Chen, F., Dudhia, J., 2001. Coupling an advanced land surface–hydrology model with the Penn State–NCAR MM5 modeling system. Part I: Model implementation and sensitivity. Mon. Weather Rev. 129, 569–585. https://journals.ametsoc.org/view/journals/mwre/129/4/1520-0493_2001_129_0569_caalsh_2.0.co_2.xml, 10.1175/1520-0493(2001)129<0569:CAALSH>2.0.CO;2.
Chen, F., Kusaka, H., Bornstein, R., Ching, J., Grimmond, C.S., Grossman-Clarke, S., Loridan, T., Manning, K.W., Martilli, A., Miao, S., Sailor, D., Salamanca, F., Taha, H., Tewari, M., Wang, X., Wyszogrodzki, A.A., Zhang, C., 2011. The integrated WRF/urban modelling system: development, evaluation, and applications to urban environmental problems. Int. J. Climatol. 31, 273–288. https://doi.org/10.1002/joc.2158.
Chow, W.T.L., Svoma, B.M., 2011. Analyses of nocturnal temperature cooling-rate response to historical local-scale urban land-use/land cover change. J. Appl. Meteorol. Climatol. 50, 1872–1883. https://journals.ametsoc.org/view/journals/apme/50/9/jamc-d-10-05014.1.xml. https://doi.org/10.1175/JAMC-D-10-05014.1.
Dudhia, J., 1989. Numerical study of convection observed during the winter monsoon experiment using a mesoscale two-dimensional model. J. Atmos. Sci. 46, 3077–3107. https://journals.ametsoc.org/view/journals/atsc/46/20/1520-0469_1989_046_3077_nsocod_2_0_co_2.xml, 10.1175/1520-0469(1989)046<3077:NSOCOD>2.0.CO;2.
EEA, 2006. Urban Sprawl in Europe: The Ignored Challenge. EEA report No 10/2006,ISSN 1725–9177. European Environment Agency. https://www.eea.europa.eu/publications/eea_report_2006_10/eea_report_10_2006.pdf.
Ezpeleta, A., Royé, D., 2021. Intensidad y duración del estrés térmico en verano en el área urbana de Madrid. Geographicalia 73, 95–113. https://doi.org/10.26754/ojs_geoph/geoph.2021735202.
Fernández García, F., López Gómez, A., López Gómez, A., 1996. La influencia del relieve en la isla de calor de Madrid: las vaguadas del Manzanares y del Abroñigal. Estudios Geográficos 57, 473–494. https://estudiosgeograficos.revistas.csic.es/index.php/estudiosgeograficos/article/view/682. https://doi.org/10.3989/egeogr.1996.i224.682.
Fernando, H.J.S., 2010. Fluid dynamics of urban atmospheres in complex terrain. Annu. Rev. Fluid Mech. 42, 365–389. https://doi.org/10.1146/annurev-fluid-121108-145459.
Gallo, K.P., Easterling, D.R., Peterson, T.C., 1996. The influence of land use/land cover on climatological values of the diurnal temperature range. J. Clim. 9, 2941–2944. http://www.jstor.org/stable/26201431.
Ganbat, G., Baik, J.J., Ryu, Y.H., 2015. A numerical study of the interactions of urban breeze circulation with mountain slope winds. Theor. Appl. Climatol. 120, 123–135. https://doi.org/10.1007/s00704-014-1162-7.
García-Palomares, J.C., 2010. Urban sprawl and travel to work: the case of the metropolitan area of Madrid. J. Transp. Geogr. 18, 197–213. https://www.sciencedirect.com/science/article/pii/S0966692309000805. https://doi.org/10.1016/j.jtrangeo.2009.05.012.
Gerland, P., Hertog, S., Wheldon, M., Kantorova, V., Gu, D., Gonnella, G., Williams, I., Zeifman, L., Bay, G., Castanheira, H., Kamiya, Y., Bassarsky, L., Gaigbe-Togbe, V., Spoorenberg, T., 2022. World Population Prospects 2022: Summary of Results.
Grimmond, S., 2007. Urbanization and global environmental change: local effects of urban warming. Geogr. J. 173, 83–88. http://www.jstor.org/stable/30113496.
Grimmond, C.S.B., Oke, T.R., 1999. Heat storage in urban areas: Local-scale observations and evaluation of a simple model. J. Appl. Meteorol. 38, 922–940. https://journals.ametsoc.org/view/journals/apme/38/7/1520-0450_1999_038_0922_hsiual_2.0.co_2.xml, 10.1175/1520-0450(1999)038<0922:HSIUAL>2.0.CO;2.
He, X., Wang, J., Feng, J., Yan, Z., Miao, S., Zhang, Y., Xia, J., 2020. Observational and modeling study of interactions between urban heat island and heatwave in Beijing. J. Clean. Prod. 247, 119169. https://www.sciencedirect.com/science/article/pii/S0959652619340399. https://doi.org/10.1016/j.jclepro.2019.119169.
Hong, S., Dudhia, J., Chen, S., 2004. A Revised Approach to Ice Microphysical Processes for the Bulk Parameterization of Clouds and Precipitation. Mon. Wea. Rev. 132, 103–120. https://doi.org/10.1175/15200493(2004)132<0103:ARATIM>2.0.CO;2.
Hou, A., Ni, G., Yang, H., Lei, Z., 2013. Numerical analysis on the contribution of urbanization to wind stilling: an example over the greater Beijing metropolitan area. J. Appl. Meteorol. Climatol. 52, 1105–1115. https://journals.ametsoc.org/view/journals/apme/52/5/jamc-d-12-013.1.xml. https://doi.org/10.1175/JAMC-D-12-013.1.
IPCC, 2021. Climate Change 2021: The Physical Science Basis. Working Group I Contribution to the Sixth Assessment Report of the Intergovernmental Panel on Climate Change. Cambridge University Press. https://doi.org/10.1017/9781009157896.
Jiménez, P.A., Dudhia, J., González-Rouco, J.F., Navarro, J., Montávez, J.P., García-Bustamante, E., 2012. A revised scheme for the WRF surface layer formulation. Mon. Weather Rev. 140, 898–918. https://journals.ametsoc.org/view/journals/mwre/140/3/mwr-d-11-00056.1.xml. https://doi.org/10.1175/MWR-D-11-00056.1.
Kottek, M., Grieser, J., Beck, C., Rudolf, B., Rubel, F., 2006. World map of the Köppen-Geiger climate classification updated. Meteorol. Z. 15, 259–263. https://doi.org/10.1127/0941-2948/2006/0130.
Landsberg, H., 1981. The Urban Climate. Academic Press.
Lauwaet, D., De Ridder, K., Saeed, S., Brisson, E., Chatterjee, F., van Lipzig, N., Maiheu, B., Hooyberghs, H., 2016. Assessing the current and future urban heat island of Brussels. Urban Clim. 15, 1–15. https://www.sciencedirect.com/science/article/pii/S2212095515300377. https://doi.org/10.1016/j.uclim.2015.11.008.
Li, D., Bou-Zeid, E., 2013. Synergistic interactions between urban heat islands and heat waves: the impact in cities is larger than the sum of its parts. J. Appl. Meteorol. Climatol. 52, 2051–2064. https://journals.ametsoc.org/view/journals/apme/52/9/jamc-d-13-02.1.xml. https://doi.org/10.1175/JAMC-D-13-02.1.
Lin, C.Y., Su, C.J., Kusaka, H., Akimoto, Y., Sheng, Y.F., Huang, J.C., Hsu, H.H., 2016. Impact of an improved WRF urban canopy model on diurnal air temperature simulation over northern Taiwan. Atmos. Chem. Phys. 16, 1809–1822. https://doi.org/10.5194/acp-16-1809-2016.
Lokoshchenko, M.A., 2014. Urban 'heat island' in Moscow. Urban Clim. 10, 550–562. https://doi.org/10.1016/j.uclim.2014.01.008.
López de Lucio, R., 2003. Transformaciones territoriales recientes en la región urbana de Madrid. Urban 8, 124–161.
Lorenzo, N., Díaz-Poso, A., Royé, D., 2021. Heatwave intensity on the Iberian Peninsula: future climate projections. Atmos. Res. 258. https://doi.org/10.1016/j.atmosres.2021.105655.
Louka, P., Belcher, S.E., Harrison, R.G., 2000. Coupling between air flow in streets and the well-developed boundary layer aloft. Atmos. Environ. 34, 2613–2621. https://doi.org/10.1016/S1352-2310(99)00477-X.
Lüthi, S., Fairless, C., Fischer, E., Scovronick, N., Armstrong, B., Coelho, M., Guo, Y.L., Guo, Y., Honda, Y., Huber, V., Kyselý, J., Lavigne, E., Royé, D., Ryti, N., Silva, S., Urban, A., Gasparrini, A., Bresch, D., Vicedo-Cabrera, A., 2023. Rapid increase in the risk of heat-related mortality. Nat. Commun. 14. https://doi.org/10.1038/s41467-023-40599-x.
Ma, X., Miao, S., Masson, V., Wurtz, J., Zhang, Y., Wang, J., Huang, X.Y., Yan, C., 2024. The synergistic effects of urbanization and an extreme heatwave event on urban thermal environment in Paris. Urban Clim. 53, 101785. https://www.sciencedirect.com/science/article/pii/S2212095523003796. https://doi.org/10.1016/j.uclim.2023.101785.

Maqueda, G., Yagüe, C., Román-Cascón, C., Serrano, E., Ander Arrillaga, J., 2020. Analysis of Temperature Trends and Urban Heat Island in Madrid, in: EGU General Assembly 2020, Online, 4–8 May 2020, EGU2020–10969. https://doi.org/10.5194/egusphere-egu2020-10969.
Martilli, A., Clappier, A., Rotach, M.W., 2002. An urban surface exchange parameterisation for mesoscale models. Bound.-Layer Meteorol. 104, 261–304. https://doi.org/10.1023/A:1016099921195.
Martilli, A., Krayenhoff, E.S., Nazarian, N., 2020. Is the Urban Heat Island intensity relevant for heat mitigation studies? Urban Clim. 31. https://doi.org/10.1016/j.uclim.2019.100541.
Miao, Y., Hu, X.M., Liu, S., Qian, T., Xue, M., Zheng, Y., Wang, S., 2015. Seasonal variation of local atmospheric circulations and boundary layer structure in the Beijing-Tianjin-Hebei region and implications for air quality. J. Adv. Model. Earth Syst. 7, 1602–1626. https://doi.org/10.1002/2015MS000522 arXiv:https://agupubs.onlinelibrary.wiley.com/doi/pdf/10.1002/2015MS000522.
Mills, G., Stewart, I.D., Niyogi, D., 2022. The origins of modern urban climate science: reflections on 'A numerical model of the urban heat island'. Prog. Phys. Geogr. 46, 649–656. https://doi.org/10.1177/03091333221107212.
Mlawer, E.J., Clough, S.A., 1997. On the Extension of Rapid Radiative Transfer Model to the Shortwave Region. https://api.semanticscholar.org/CorpusID:17274414.
Monin, A.S., Obukhov, A.M., 1954. Basic laws of turbulent mixing in the surface layer of the atmosphere. Contrib. Geophys. Inst. Acad. Sci. USSR 151, e187.
Muñoz, F., 2003. Lock living: urban sprawl in mediterranean cities. Cities 20, 381–385. https://www.sciencedirect.com/science/article/pii/S0264275103000738. https://doi.org/10.1016/j.cities.2003.08.003. part Special Issue: Cities of Spain.
Myrup, L.O., 1969. A numerical model of the urban heat island. J. Appl. Meteorol. Climatol. 8, 908–918. https://journals.ametsoc.org/view/journals/apme/8/6/1520-0450_1969_008_0908_anmotu_2_0_co_2.xml, 10.1175/1520-0450(1969)008<0908:ANMOTU>2.0.CO;2.
National Institute of Statistics of Spain, 2023. Official Population Figures of Spanish Municipalities in Accordance with the Local Government Base Law (Art. 17). Population by municipalities and gender, Madrid. https://www.ine.es/jaxiT3/Tabla.htm?t=2881&L=0.
Núñez-Peiró, M., Sánchez-Guevara Sánchez, C., Neila González, F.J., 2021. Hourly evolution of intra-urban temperature variability across the local climate zones. The case of Madrid. Urban Clim. 39, 100921. https://www.sciencedirect.com/science/article/pii/S2212095521001516. https://doi.org/10.1016/j.uclim.2021.100921.
Oke, T., 1973. City size and the urban heat island. Atmos. Environ. 7, 769–779 (1967). https://www.sciencedirect.com/science/article/pii/0004698173901406. https://doi.org/10.1016/0004-6981(73)90140-6.
Oke, T.R., 1988. The urban energy balance. Prog. Phys. Geogr. 12, 471–508. https://doi.org/10.1177/030913338801200401.
Oke, T.R., Cleugh, H.A., 1987. Urban heat storage derived as energy balance residuals. Bound.-Layer Meteorol. 39, 233–245. https://doi.org/10.1007/BF00116120.
Oke, T.R., Mills, G., Christen, A., Voogt, J.A., 2017. Urban Climates. Cambridge University Press. https://www.cambridge.org/core/product/identifier/9781139016476/type/book. https://doi.org/10.1017/9781139016476.
Rasilla, D., Allende, F., Martilli, A., Fernández, F., 2019. Heat waves and human well-being in Madrid (Spain). Atmosphere 10. https://doi.org/10.3390/atmos10050288.
Román-Cascón, C., Yagüe, C., Arrillaga, J., Lothon, M., Pardyjak, E., Lohou, F., Inclán, R., Sastre, M., Maqueda, G., Derrien, S., Meyerfeld, Y., Hang, C., Campargue-Rodríguez, P., Turki, I., 2019. Comparing mountain breezes and their impacts on CO2 mixing ratios at three contrasting areas. Atmos. Res. 221, 111–126. https://www.sciencedirect.com/science/article/pii/S0169809519300596. https://doi.org/10.1016/j.atmosres.2019.01.019.
Román-Cascón, C., Yagüe, C., Ortiz-Corral, P., Serrano, E., Sánchez, B., Sastre, M., Maqueda, G., Alonso-Blanco, E., Artiñano, B., Gómez-Moreno, F., Diaz-Ramiro, E., Fernández, J., Martilli, A., FerGarcía, A., Núñez, A., Cordero, J., Narros, A., Borge, R., 2023. Wind and turbulence relationship with NO2 in an urban environment: a fine-scale observational analysis. Urban Clim. 51, 101663. https://www.sciencedirect.com/science/article/pii/S2212095523002572. https://doi.org/10.1016/j.uclim.2023.101663.
Rotach, M.W., 1993. Turbulence close to a rough urban surface part I: Reynolds stress. Bound.-Layer Meteorol. 65, 1–28. https://doi.org/10.1007/BF00708816.
Sailor, D.J., 2011. A review of methods for estimating anthropogenic heat and moisture emissions in the urban environment. Int. J. Climatol. 31, 189–199. https://doi.org/10.1002/joc.2106.
Salamanca, F., Krpo, A., Martilli, A., Clappier, A., 2010. A new building energy model coupled with an urban canopy parameterization for urban climate simulations-part I. Formulation, verification, and sensitivity analysis of the model. Theor. Appl. Climatol. 99, 331–344. https://doi.org/10.1007/s00704-009-0142-9.
Salamanca, F., Martilli, A., Yagüe, C., 2012. A numerical study of the Urban Heat Island over Madrid during the DESIREX (2008) campaign with WRF and an evaluation of simple mitigation strategies. Int. J. Climatol. 32, 2372–2386. https://doi.org/10.1002/joc.3398.
Salamanca, F., Georgescu, M., Mahalov, A., Moustaoui, M., Wang, M., Svoma, B.M., 2013. Assessing summertime urban air conditioning consumption in a semiarid environment. Environ. Res. Lett. 8. https://doi.org/10.1088/1748-9326/8/3/034022.
Santiago, J., Martilli, A., Martin, F., 2007. CFD simulation of airflow over a regular array of cubes. Part I: Three-dimensional simulation of the flow and validation with wind-tunnel measurements. Bound.-Layer Meteorol. 122, 609–634. https://doi.org/10.1007/s10546-006-9123-z.
Schlünzen, K.H., Grimmond, S., Baklanov, A., 2023. Guidance to measuring, modelling and monitoring the canopy layer urban heat island. In: EMS Annual Meeting 2021, online, 6–10 Sep 2021, EMS2021–301. https://doi.org/10.5194/ems2021-301.
Sharma, A., Wuebbles, D.J., Kotamarthi, R., Calvin, K., Drewniak, B., Catlett, C.E., Jacob, R., 2020. Urban scale processes in high spatial resolution earth system models (ESMs). Bull. Am. Meteorol. Soc. https://doi.org/10.1175/BAMS-D-20-0114.1.
Stewart, I.D., Oke, T.R., 2012. Local climate zones for urban temperature studies. Bull. Am. Meteorol. Soc. 93, 1879–1900. https://doi.org/10.1175/BAMS-D-11-00019.1.
Tewari, M., Salamanca, F., Martilli, A., Treinish, L., Mahalov, A., 2017. Impacts of projected urban expansion and global warming on cooling energy demand over a semiarid region. Atmos. Sci. Lett. 18, 419–426. https://doi.org/10.1002/asl.784.
Tobias, A., Royé, D., Iñiguez, C., 2023. Heat-attributable mortality in the summer of 2022 in Spain. Epidemiology (Cambridge, Mass.) 32, 5–6. https://doi.org/10.1097/EDE.0000000000001583.
Uhl, J.H., Royé, D., Burghardt, K., Aldrey Vázquez, J.A., Borobio Sanchiz, M., Leyk, S., 2023. HISDAC-ES: historical settlement data compilation for Spain (1900–2020). Earth Syst. Sci. Data 15, 4713–4747. https://essd.copernicus.org/articles/15/4713/2023/. https://doi.org/10.5194/essd-15-4713-2023.
Vicedo-Cabrera, A., Scovronick, N., Sera, F., Royé, D., Schneider, R., Tobias, A., Åström, C., Guo, Y., Honda, Y., Hondula, D., Abrutsky, R., Tong, S., Sousa, M., Coelho, Z., Saldiva, P., Lavigne, E., Correa, P., Valdes Ortega, N., Kan, H., Holobaca, I., 2021. The burden of heat-related mortality attributable to recent human-induced climate change. Nat. Clim. Chang. 182. https://doi.org/10.1038/s41558-021-01058-x.
Vitanova, L.L., Kusaka, H., Doan, Q.V., Subasinghe, S., 2021. How urban growth changes the heat island effect and human thermal sensations over the last 100 years and towards the future in a European city? Meteorol. Appl. 28, e2019. https://doi.org/10.1002/met.2019 arXiv:https://rmets.onlinelibrary.wiley.com/doi/pdf/10.1002/met.2019.
Wang, J., Feng, J., Yan, Z., Hu, Y., Jia, G., 2012. Nested high-resolution modeling of the impact of urbanization on regional climate in three vast urban agglomerations in China. J. Geophys. Res.-Atmos. 117. https://doi.org/10.1029/2012JD018226 arXiv:https://agupubs.onlinelibrary.wiley.com/doi/pdf/10.1029/2012JD018226.
Wouters, H., De Ridder, K., Demuzere, M., Lauwaet, D., van Lipzig, N.P.M., 2013. The diurnal evolution of the urban heat island of Paris: a model-based case study during summer 2006. Atmos. Chem. Phys. 13, 8525–8541. https://acp.copernicus.org/articles/13/8525/2013/. https://doi.org/10.5194/acp-13-8525-2013.
Yagüe, C., Zurita, E., Martinez, A., 1991. Statistical analysis of the Madrid urban heat island. Atmos. Environ. B. Urban Atmos. 25, 327–332. https://www.sciencedirect.com/science/article/pii/095712729190004X. https://doi.org/10.1016/0957-1272(91)90004-X.
Yan, Z.W., Wang, J., Xia, J.J., Feng, J.M., 2016. Review of recent studies of the climatic effects of urbanization in China. Adv. Clim. Chang. Res. 7, 154–168. https://www.sciencedirect.com/science/article/pii/S1674927816300211. https://doi.org/10.1016/j.accre.2016.09.003. including special topic on atmospheric black carbon and its effects on cryosphere.
Yu, B., Zhu, B., Miao, S., Kang, H., He, X., Liu, H., Liang, Z., Chen, F., 2021. Observational signal of the interaction between mountain–plain wind and urban breeze under weak synoptic systems. J. Geophys. Res.-Atmos. 126. https://doi.org/10.1029/2020JD032809 e2020JD032809. arXiv:https://agupubs.onlinelibrary.wiley.com/doi/pdf/10.1029/2020JD032809.

Zhang, G.J., Cai, M., Hu, A., 2013. Energy consumption and the unexplained winter warming over northern Asia and North America. Nat. Clim. Chang. 3, 466–470. https://doi.org/10.1038/nclimate1803.

Zhao, L., Oppenheimer, M., Zhu, Q., Baldwin, J.W., Ebi, K.L., Bou-Zeid, E., Guan, K., Liu, X., 2018. Interactions between urban heat islands and heat waves. Environ. Res. Lett. 13. https://doi.org/10.1088/1748-9326/aa9f73.

Zhou, B., Rybski, D., Kropp, J.P., 2017. The role of city size and urban form in the surface urban heat island. Sci. Rep. 7. https://doi.org/10.1038/s41598-017-04242-2.

Zhu, X., Ni, G., Cong, Z., Sun, T., Li, D., 2016. Impacts of surface heterogeneity on dry planetary boundary layers in an urban-rural setting. J. Geophys. Res. 121, 12,164–12,179. https://doi.org/10.1002/2016JD024982.